# Synchronization Performance of IEEE 802.15.4 IR-UWB Systems in Industrial Environments

Rafael Reinhold, *Student Member, IEEE*, and Ruediger Kays, *Senior Member, IEEE*

***Abstract*— Wireless sensor networks for industrial communication require both low latency and high reliability. As state of the art wireless sensor networks do not entirely meet these requirements, novel system approaches need to be developed. In this regard, ultra wideband communication systems seem to be a promising approach due to the high bandwidth and the robustness against frequency selectivity. This paper analyzes the IEEE 802.15.4 impulse-radio ultra-wideband physical layer in industrial environments. The performance is evaluated based on the IEEE 802.15.4a channel model as well as on channel measurement campaigns, which have been performed in realistic environments. The analysis in terms of packet error rate and coverage range considers the impact of two synchronization procedures. The results show a significant influence on the frequency selectivity. This work may serve as a guideline for the development of an industrial wireless sensor network.**

***Index Terms*— channel measurement, IEEE 802.15.4, industrial environments, IR-UWB, performance evaluation, ultra-wideband, wireless sensor networks.**

## I. Introduction

In the area of industrial communication, wireless sensor networks gain increasing importance due to the advantages regarding retrofitting, flexibility and mobility. Nevertheless, the severe frequency selectivity of channels in industrial environments is a very demanding task. Critical environments with multipath propagation and fast channel variations lead to packet errors and high latencies when conventional solutions are applied. To overcome these performance degradations, novel solutions have to be developed. Impulse-radio ultra-wideband (IR-UWB) seems to be a promising system approach due to its huge bandwidth, the operation at sparsely used frequency bands and the robustness against frequency fading. The system bandwidth of nearly 500 MHz results from transmitting short impulses of approximately 2 ns. The Electronic Communications Committee (ECC) has regulated the operating frequency band, which ranges from 3.1 to 10.6 GHz. The average power density of -41.3 dBm/MHz and the maximal power density of 0 dBm / 50 MHz have been limited [1]. On one side, the low power operation improves the coexistence with neighboring systems as well as facilitates the development of battery driven devices. On the other side, the coverage range is limited.

Part of the research leading to these results has received funding from the German Federal Ministry of Education and Research under grant agreement no. 16BU1222 also referred to as KUSZ.

This paper analyzes the performance in terms of packet error rate and coverage range of the IR-UWB system in industrial environments. Based on channel measurements, the impact of the synchronization procedure is included in the investigation.

The structure of this paper is as follows. Section II gives an overview on the IEEE 802.15.4 IR-UWB PHY. Section III describes the implemented synchronization procedures. Next, the channel measurements in industrial environments, which provide the basis for evaluation, are summarized. The evaluation methodology is described in section V. The following section presents the evaluation results. Finally, section VII concludes this paper.

## II. IEEE 802.15.4-2011 IR-UWB PHY

In the IR-UWB PHY standard [2], data rates from 0.11 to 27.24 Mb/s are specified. There are three different operating bands defined: sub-gigahertz band (249.6 MHz to 749.6 MHz), low band (3.1 GHz to 4.8 GHz), and high band (5.8 GHz to 10.6 GHz). Due to regulatory restrictions such as power limitation and duty cycle, the high band with a mandatory channel at 7.9872 GHz is selected for evaluation.

The UWB impulses of PHR and PSDU are modulated by means of a combination of binary phase shift keying (BPSK) and burst position modulation (BPM). The BPM-BPSK modulation scheme carries two bits of information in each UWB symbol. Whereas the first bit defines the burst position, the second bit is encoded in the burst's polarity. A burst itself consists of a distinct number of single impulses. The sign of the individual impulses is determined by a pre-defined spreading code. The UWB PHY symbol structure is shown in Fig. 1. $T_{dsym}$ equals the total symbol duration, $T_c$ the chip duration and $N_{cpb}$ the number of chips per burst.

The UWB PHY deploys a concatenation of an outer Reed Solomon $RS_6(63,55)$ systematic block code and an inner convolutional code (CC) for payload protection ($R_{CC}$ = ½, $g_0$ =

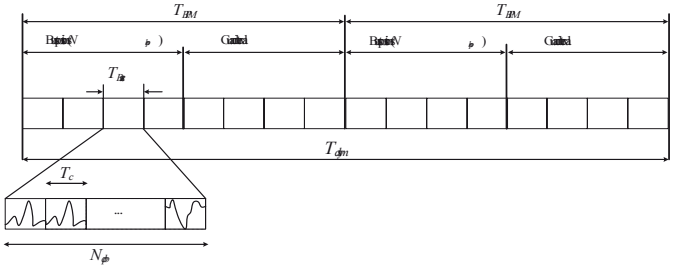

Fig. 1. IEEE 802.15.4a IR-UWB PHY symbol structure.

ISBN 978-3-8007-3585-3

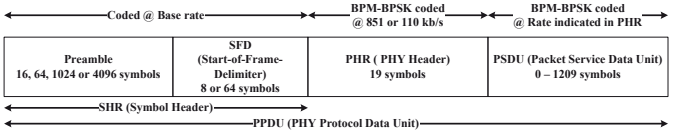


Fig. 2. IEEE 802.15.4a PPDU structure.

$[010]_2$, $g_1 = [101]_2$). The PHY Header (PHR) is protected by a modified Hamming code (SECDEC - single error correct, double error detect) as well as the above mentioned RS code.

The PHY protocol data unit (PPDU) is divided into the symbol header (SHR), the PHY header (PHR) and the data field. The SHR enables synchronization and clock recovery. It is separated into a preamble and a start of frame delimiter (SFD). Both the preamble and SFD lengths are adjustable according to reliability requirements. In this paper, the SHR with a duration of 23.8 µs has been selected. The IR-UWB signal processing chain is summarized in Fig. 2.

The IR-UWB PHY offers a large number of parameters to adapt to different communication scenarios. The mandatory modulation coding scheme (MCS) 2 with a data rate of 0.85 Mb/s is investigated. The rate of the CC code equals 0.5 and the rate of the RS code is 0.87. A burst length of 16 is defined. MCS 2 uses 8 hopping positions and 32 burst positions per symbol. The resulting BPM-BPSK symbol duration equals 1025.64 ns, and the occupied bandwidth is 499.2 MHz.

## III. Synchronization Procedures

When using a BPM-BPSK modulation especially under conditions of multipath fading, a precise synchronization is essential. We have investigated two different synchronization procedures.

The first synchronization (Sync 1) is realized in two steps. The received signal is correlated with the coefficients of the preamble symbol. The correlation $R_1$ of the first synchronization step is given in the following equation:

$$R_1(t) = \sum_{n=0}^{N-1} x(t+n) \cdot p_{sym}{}^*(t) \tag{1}$$

$N$ describes the number of samples of a preamble symbol, $x$ the baseband input signal and $p_{sym}$ the template of the preamble symbol. In a second step, $R_1$ is correlated with the SFD to detect the start of the PHR. As shown in [2], the SFD detection probability increases if three more preamble symbols are added to the correlation sequence. Equation (2) defines the correlation $R_1$ of the second step of the synchronization.

$$R_2(t) = \sum_{m=0}^{M-1} R_1(t+m) \cdot SFD_{extended}{}^*(t) \tag{2}$$

$M$ describes the number of samples of the extended SFD and $SFD_{extended}$ the template of the extended SFD samples.

Finally, a maximum decision is performed and the corresponding sample index is assumed as the begin of the PHR. Since the correlation bases on the coefficients of the preamble symbols, the resolution of this procedure is 2 ns.

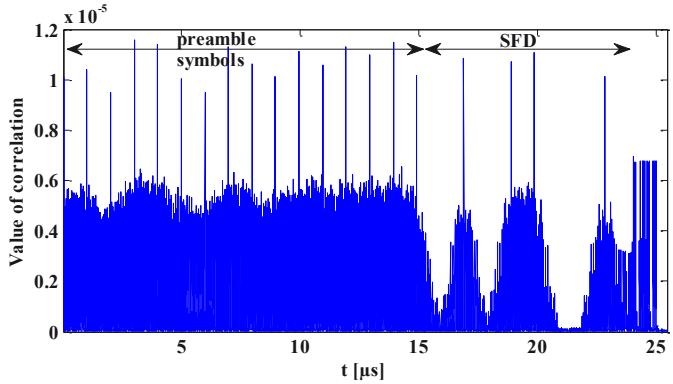


Fig. 3. First synchronization step of Sync 1 *(S/N* = 6 dB, LOS 3 m).

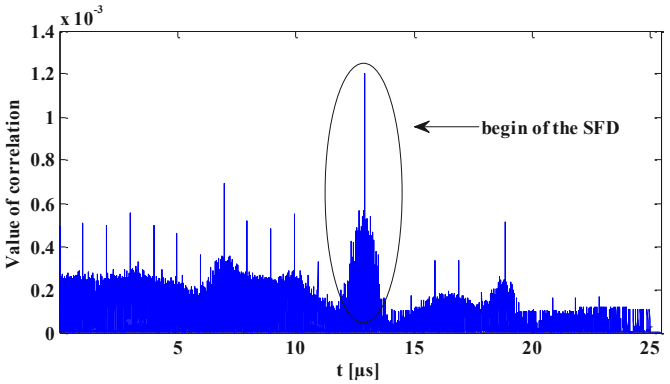


Fig. 4. Second synchronization step of Sync 1 *(S/N* = 6 dB, LOS 3 m).

Both synchronization steps are illustrated in Fig. 3 and 4, where the values of the correlation are plotted versus the time. In Fig. 3, the characteristic peaks of the local maxima of the correlation can be seen, which are ideally spaced at an interval of the duration of a preamble symbol. In the second step, the position of the SFD is found by maximum decision, as pictured in Fig. 4.

The second synchronization procedure (Sync 2) seizes the work in [3], where the correlation is based on blocks with a duration of 32 ns. The block duration result from the energy detector with a detection window of the same duration. Here, the received signal ($d$) is correlated with the preamble coefficients ($c$), as depicted in (3). Each preamble symbol consists of 31 coefficients.

$$corr(d,c) = \sum_{k=0}^{30} d_k \cdot (2 \cdot c_k - 1) \tag{3}$$

In the next step, the maximum of every consecutive block containing 31 results of the correlation ($corr$) is determined. A preamble is assumed to be successfully detected if the last 8 indices of the maximum value have the same periodicity. Finally, the SFD is detected by comparing with the SFD pattern, which is extended by the previous three symbols. If at least 10 of 11 symbols match, the SFD is assumed to be detected. Additional details on this synchronization procedure may be found in [3].

ISBN 978-3-8007-3585-3

## IV. CHANNEL MEASUREMENTS

Frequency domain measurements with the vector network analyser (VNA) in the range of 6 to 8.5 GHz have been performed in representative industrial environments. Both scenarios with LOS (3 and 8 m) and NLOS (10 m) have been chosen in a factory building characterized by a high number of reflective obstacles. An antenna positioner has been used to average the effect of spatial correlation. Since the location of measurement points should be spaced at most λ/2 apart [4], we chose 1 cm.

In order to revert the impact of the measurement setup, a calibration measurement in an anechoic chamber (AC) has been carried out. Transmitter and receiver antenna (A), antenna cables (C), network analyzer including the front end (FE) and the interfaces of components influence the measurement ($H_{VNA}(f) = H_{FE}(f) \cdot H_C(f) \cdot H_A(f) \cdot H_{CTF}(f)$). $H_{CTF}^*$ equals the calibrated CTF, which is an approximation of the acutal $H_{CTF}$. $H_{CTF}^*$ is interpreted as complex baseband channel transfer function, as given in (4).

$$H_{CTF}^*(f) = \frac{H_{FE}(f) \cdot H_c(f) \cdot H_A(f) \cdot H_{CTF}(f)}{H_{VNA\,AC}(f) \cdot \exp(j \cdot 2\pi \cdot f \cdot t_{ref} / c_{air}) \cdot a_{ref}} \quad (4)$$

$t_{ref}$ and $a_{ref}$ correspond to the delay and the attenuation regarding the reference distance between transmitter and receiver antenna (42.5 cm). The effective receiver bandwidth of the VNA was set to 10 Hz. Since 10 iterations have been performed per measurement position (100), the resulting noise floor can be reduced further by averaging. Fig. 5 shows a snapshot of the transfer functions of the 7.9872 GHz channel in the NLOS scenario. This channel is mandatory to be implemented and has a bandwidth of 499.2 MHz. The transfer functions are characterized by a high number of deep fades indicating a high frequency selectivity. The mean rms delay spread ($\sigma_{rms}$) is 17.8 ns in case of LOS 3 m, 31 ns in case of NLOS 10 m and 25.7 ns in case of LOS 8 m.

## V. EVALUATION METHODOLOGY

The PHY evaluation is based on a standard-compliant implementation of the IEEE 802.15.4-2011 IR-UWB PHY in MATLAB. In this paper, the performance of MCS 2 in case of an energy detection receiver is evaluated. To compare the performance under realistic channel conditions, we used the results of our measurements as well as the IEEE 802.15.4a channel model [5] at 7.9 GHz. Both industrial LOS (CM7) and NLOS (CM8) environments with $\sigma_{rms}$ of 8.7 ns and 89.2 ns have been selected. Based on simulation results in terms of packet error rate (PER) and signal-to-noise ratio (*S/N*), the resulting coverage range has been derived [6]. In equation (5), the coverage range $d_{dB}$ is connected to *S/N,* which is derived from system simulations.

$$d_{dB} = G_{TX} + G_{RX} - F - I - 20 \cdot \log_{10}(f_c) - 92.44 + P_{TX} - P_N - S/N_{dB} \quad (5)$$

$G_{TX}$ and $G_{RX}$ denote the antenna gain of transmitter and receiver antenna respectively. $F$ equals the noise figure and $I$ the implementation losses. $f_c$ describes the carrier frequency given in GHz and $d$ the distance between sender and transmitter, given in kilometer (coverage range). $P_{TX}$ and $P_{RX}$ represent transmission and reception power respectively. $P_N$ is referred to as the noise power.

For system evaluation, no antenna gains have been assumed to enable a general-purpose analysis. Moreover, an implementation loss of 10 dB, a noise figure of 4.6 dB [7] and an effective antenna temperature of 290 K have been set. The maximal permitted equivalent isotropically radiated power has been chosen.

The exemplary application payload length used for system evaluation was set to 48 Byte, which represents a suitable mean value for industrial wireless sensor networks. The MAC header was set to 9 Byte and the PHY header has a fixed size of 19 Bit.

## VI. EVALUATION RESULTS

The simulation results have been obtained up to a PER of $10^{-4}$. Due to the usage of RS codes, the PER can be extrapolated towards smaller PERs. The PER performance is presented in Fig. 6. Generally, the impact of the multipath

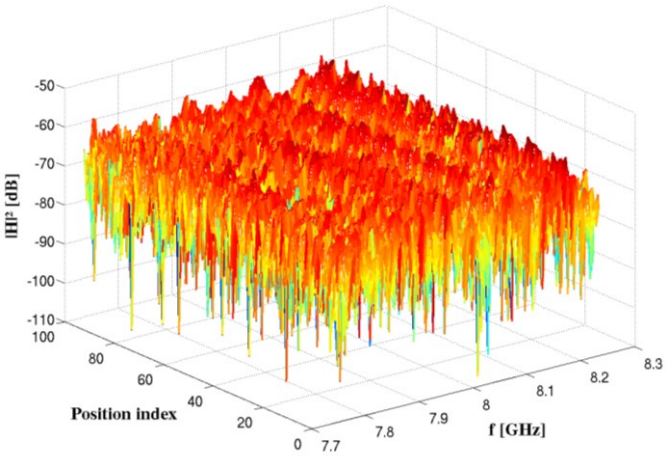


Fig. 5. Transfer function of the 7.9872 GHz channel (NLOS 10 m).

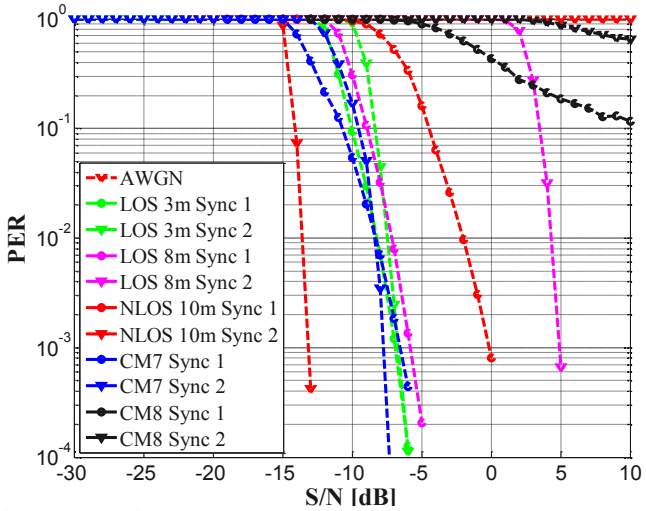


Fig. 6. PER performance of MCS2 versus S/N.

ISBN 978-3-8007-3585-3

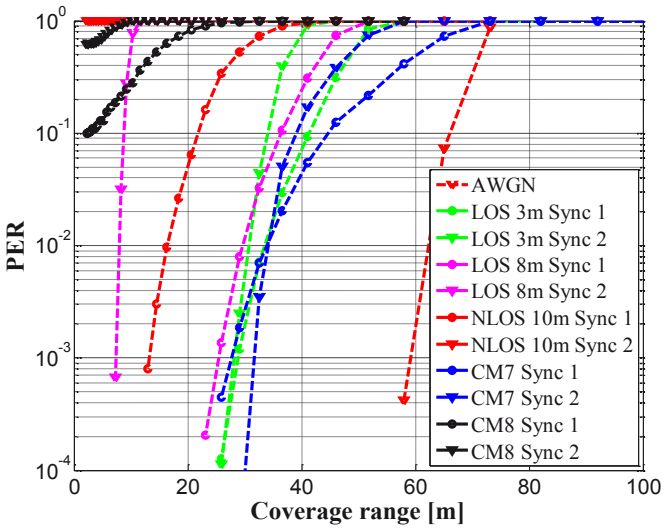


Fig. 7. PER performance of MCS2 versus coverage range.

propagation leads to a performance degradation between 7 and 18 dB at a PER of $10^{-3}$. Whereas the performance of both synchronization procedures is comparable for CM7 and LOS 3 m, Sync 1 outperforms Sync 2 with increasing frequency selectivity (LOS 8 m, NLOS). Both procedures fail in case of CM8, which is characterized by the highest delay spread. CM8, which bases on a tapped delay line model produces impulse responses, which lead to a very high spread of the received signal and to a significant attenuation of the first multipath component. The energy detector fails, since the spread of the received energy strongly exceeds the detection window.

Next, the impact of the synchronization procedure on the coverage range is analyzed. In Fig. 7, the PER performance of MCS 2 versus the coverage range is shown. The resulting maximum operating distances are 60 m (AWGN), 25 - 32 m (LOS) and 12 m (NLOS) at a PER of $10^{-3}$. With the increase of frequency selectivity, the coverage range reduces strongly. Whereas environments with transfer functions of moderate frequency selectivity enable a reliable communication up to approximately 30 m, NLOS environments limit the communication range to less than 12 m. As applications in the domain of factory automation require a coverage range of 20 m [8], an extract of the results only meets this requirement. Moreover, the choice of the synchronization procedure significantly influences the system usability. In case of using Sync 2 for LOS 8 m, the achieved coverage range of 7 m disqualifies the system for many applications within the area of industrial communication. Sync 2, which is a tradeoff between complexity and accuracy, performs poorly with increasing $\sigma_{rms}$ due to the coarse resolution.

The results reveal a severe impact on the frequency selectivity. Thus, the synchronization has still to be improved to meet the demands of industrial communication. The requirements on the synchronization are even increased in case of coherent reception [9].

## VII. Conclusion

In this paper, channel measurements of representative industrial environments have been presented. Based on both measurements and the IEEE 802.15.4a channel model, the performance of the IR-UWB PHY in case of an energy detector has been analyzed. Two synchronization procedures have been considered in the evaluation. Sync 1 bases on the coefficients of the preamble symbols and is characterized by a resolution of 2 ns. Sync 2 bases on blocks with a duration of 32 ns and yields a trade-off between complexity and synchronization accuracy. Even with MCS 2, which offers a relatively low data rate, the performance is strongly reduced when operating in highly reflective environments. Whereas a performance degradation of at least 7 dB is observed in a 3 m LOS scenario, at least 13 dB is denoted at 10 m NLOS. With a further increase of the frequency selectivity (CM8), both synchronization procedures fail. Moreover, coverage ranges of maximal 7 m are achieved by MCS2 in case of NLOS. The evaluation results reveal the necessity to improve the synchronization procedures.

Further steps will include enhancements of the physical layer to increase system reliability. Besides the optimization of synchronization procedures, the dynamic adaption of the detection window to the delay spread of the channel seems to be a promising approach. The investigations will focus on implementations with moderate complexity. In addition, measurements of transmission channels with memory will be performed. Particularly in environments of factory automation, certain movements are repeated periodically. In a next step, the characteristics of cyclic transmission channels are studied in order to derive system adaptations and improvements respectively.

## References

[1] Electronic Communications Committee (ECC): Decision of 24 March 2006 on the harmonised conditions for devices using Ultra-Wideband (UWB) technology in bands below 10.6 GHz (ECC/DEC/(06)04), Mar. 2006.

[2] IEEE Std 802.15.4-2011: Part 15.4: Low-Rate Wireless Personal Area Networks (LR-WPANs), Sep. 2011.

[3] D. Kreiser and S. Olonbayar, "Efficient Synchronization Method for IR-UWB 802.15.4a non-coherent Energy Detection Receiver," in Green Computing and Communications, pp.521-526, Dec. 2010.

[4] H. Krim and M. Viberg, B, "Two decades of array signal processing research," IEEE Signal Process. Mag., pp. 67–93,1996.

[5] A. F. Molisch et al.: IEEE 802.15.4a channel Model - Final report, Tech. Rep. Doc. IEEE 802.15-04-0662-02-004a, 2005.

[6] R. Reinhold, "Coverage Range Analysis of IEEE 802.15.4a IR-UWB for Reliable Data Transmission in Wireless Sensor Netowks," in 2nd IEEE International Workshop M&N 2013, Naples, Oct. 2013.

[7] G. Fischer, K. Oleksiy, and D. Martynenko, "Time-of-Arrival measurement extension to a non-coherent impulse radio UWB transceiver," in 5th Workshop on Positioning, Navigation and Communication (WPNC), 2008, pp. 265-270.

[8] ZVEI: Automation, "Coexistence of Wireless Systems in Automation Technology," Technical Report, ZVEI – German Electrical and Electronic Manufacturers Association, Apr. 2009.

[9] H. Arslan, Zhi Ning Chen and M.-G. Di Benedetto, Ultra wideband wireless communication, Wiley-Interscience, 2006.

ISBN 978-3-8007-3585-3